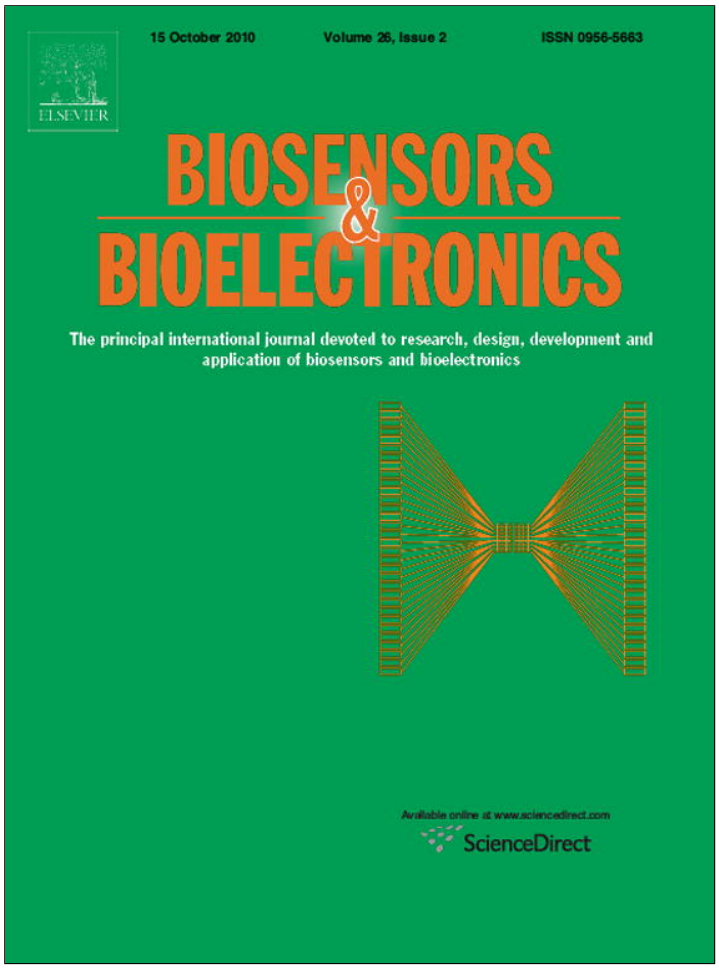

Biosensors and Bioelectronics 26 (2010) 371–376

Contents lists available at ScienceDirect

Biosensors and Bioelectronics

journal homepage: www.elsevier.com/locate/bios

Highly sensitive electrocatalytic biosensing of hypoxanthine based on functionalization of graphene sheets with water-soluble conducting graft copolymer

Jing Zhang, Jianping Lei, Rong Pan, Yadong Xue, Huangxian Ju*

Key Laboratory of Analytical Chemistry for Life Science (Ministry of Education of China), Department of Chemistry, Nanjing University, Nanjing 210093, PR China

ARTICLE INFO

Article history:
Received 2 June 2010
Received in revised form 24 July 2010
Accepted 30 July 2010
Available online 7 August 2010

Keywords:
Graphene
Conducting graft copolymer
Functionalization
Electrocatalysis
Biosensing

ABSTRACT

A novel electrocatalytic biosensing platform was designed by the functionalization of reduced graphene oxide sheets (RGO) with conducting polypyrrole graft copolymer, poly(styrenesulfonic acid-g-pyrrole) (PSSA-g-PPY), via π–π noncovalent interaction. The resulting nanocomposite could well disperse in water for at least 2 months with a solubility of 3.0 mg mL^{-1}. The nanocomposite was characterized with atomic force microscopy, X-ray photoelectron spectroscopy, ultraviolet–visible absorption, contact angle measurement, and electrochemical impedance spectroscopy. Based on the advantageous functions of PSSA-g-PPY and RGO, the functional nanocomposite modified platinum electrode showed high electrocatalytic activity toward the oxidation of hydrogen peroxide and uric acid in neutral media. Further, a hypoxanthine biosensor was constructed by combining the modified electrode with the enzymatic reaction of xanthine oxidase. The biosensor exhibited a wide linear response ranging from 3.0×10^{-8} to 2.8×10^{-5} M with a high sensitivity of 673 ± 4 μA M^{-1} cm^{-2}. The detection limit of 10 nM at a signal-to-noise ratio of 3 was one order of magnitude lower than that reported previously. The assay results of hypoxanthine in fish samples were in a good agreement with the reference values. The water-soluble conducting copolymer could serve as an efficient species for functionalization and solubilization of graphene sheets in biosensing and biocatalytic applications.

1. Introduction

Graphene, as an atomic-layer-thick 2D system, has recently emerged as an intriguing material for potential applications in nanoelectronics, biomedicines and sensors due to its unique mechanical and electronic properties (Stankovich et al., 2006a; Yang et al., 2008; Geim, 2009; Kang et al., 2009; Li et al., 2009; Rao et al., 2009; Zhou et al., 2009; Kim et al., 2010; Shan et al., 2010; Zhong et al., 2010). Compared with other kinds of carbon materials, graphene has higher surface area and more excellent electrical conductivity (Stankovich et al., 2006a; Kang et al., 2009), which provides insight to fabricate sensitive biosensors in practice (Du et al., 2010). Although reducing exfoliated graphene oxide (GO) has become a good way to produce graphene (Stankovich et al., 2007; Robinson et al., 2008), the reduced graphene oxide (RGO) is prone to aggregate when reducing GO in water using reductant without additional reagent. The poor dispersion remains one major drawback for its applications. A number of strategies, such as chemical modifications (Li et al., 2008a; Si and Samulski, 2008; Yang et al., 2009; Zhu et al., 2009) and noncovalent functionalizations (Xu et al., 2008; Patil et al., 2009; Subrahmanyam et al., 2009; Liu et al., 2010), have been explored for their solubilization and the subsequent fabrication of nanocomposite materials. The noncovalent functionalization can avoid destruction of π-conjugated skeleton and loss of electronic properties of the graphene. Thus some polymers have been used for these purposes by conjugation with the planar structure of the graphene (Stankovich et al., 2006b; Li et al., 2008b; Wang et al., 2009).

Of a wide range of polymer materials, conducting polymers exhibit great potential as efficient sensing elements in virtue of their excellent electrical and optical properties (Kong et al., 2003; Widge et al., 2007; Holcombe et al., 2009; Yoon and Jang, 2009). In order to improve the solubility of graphene sheets, sulfonated polyaniline has been induced in the reduction of GO for the electrocatalysis of ascorbic acid oxidation (Bai et al., 2009). The RGO has been also functionalized with polythiophene derivatives for the preparation of photovoltaic cells (Liu et al., 2009b). Although the electrical conductivity of polypyrrole (PPY) is roughly 10 times higher than that of polyaniline (Bae et al., 2005), it has not been used for functionalization of graphene due to the inherent poor solubility of PPY in common solvents, which originates from the strong inter- and intra-chain interactions. This feature has

* Corresponding author. Tel.: +86 25 83593593; fax: +86 25 83593593.
E-mail address: hxju@nju.edu.cn (H. Ju).

0956-5663/$ – see front matter © 2010 Elsevier B.V. All rights reserved.
doi:10.1016/j.bios.2010.07.127

also greatly limited its practical application in many areas (Chao and Wrighton, 1987). This work used a polypyrrole graft copolymer, poly(styrenesulfonic acid-g-pyrrole) (PSSA-g-PPY), which is of good water-solubility and high conductivity due to combining the features of different monomers (Bae et al., 2005), to functionalize RGO via π–π noncovalent interaction. The PSSA-g-PPY functionalized RGO nanocomposite showed good dispersion in water, high electrical conductivity, and excellent electrocatalytic activity for biosensing application. Thus a novel biosensor for hypoxanthine was constructed.

Hypoxanthine is an essential metabolite to degrade adenine nucleotide, which is mainly accumulated in biological tissues. The determination of hypoxanthine is very important for the quality control of fish products in food industries. The analytical techniques for hypoxanthine detection usually involve chromatography and capillary electrophoresis (Causse et al., 2007; Farthing et al., 2007). However, these methods require relatively expensive equipment, advanced technical expertise, and more time-consuming. Electrochemical techniques, especially amperometric biosensors, have been considered as the best candidates for the in situ detection of hypoxanthine due to the high sensitivity, simplicity, and easy to miniaturization (Venugopal, 2002). Here, the designed PSSA-g-PPY/RGO was used for biosensing of hypoxanthine. The PSSA-g-PPY/RGO modified electrode exhibited high electrocatalytic activity toward the oxidation of hydrogen peroxide (H_2O_2) and uric acid (UA). The latter is a product of purine nucleotide metabolism and considered as a key biomarker in the evaluation of physiological conditions. Based on the electrocatalytic response to H_2O_2 and UA produced from the enzymatic reaction of xanthine oxidase (XnOx) with its substrate hypoxanthine, the proposed biosensor for hypoxanthine showed good performance with high sensitivity, wide linear range and excellent stability. It could be successfully applied in the detection of hypoxanthine in fish samples. The functionalization of RGO with water-soluble conducting copolymer provided an efficient strategy for functionalization and solubilization of graphene sheets, and broadened the application of RGO and copolymer in biosensing.

2. Experimental

2.1. Materials and reagents

Graphene oxide was prepared according to a modified Hummer's method (Hummers and Offeman, 1958). Pyrrole, xanthine oxidase (EC 1.1.3.22, from microbial source, 8.1 U mg^{-1}), poly(diallyldimethylammonium chloride) (PDDA, 20%, w/w in water, MW: 200,000–350,000) were obtained from Sigma–Aldrich Inc (USA). Potassium hydride (KH) and sodium styrenesulfonate (SSNa) were from Alfa Aesar China Ltd. Chloromethylstyrene (CMS) was from TCI (Japan). Graphite power and sodium borohydride were from Sinopharm Chemical Reagent Co. Ltd (China). All other reagents were of analytical grade. All aqueous solutions were prepared using ultra-pure water (≥18 MΩ, Milli-Q, Millipore). The buffer for assay was 0.05 M phosphate buffer saline (PBS) prepared by mixing stock-standard solutions of Na_2HPO_4 and NaH_2PO_4.

2.2. Apparatus

The morphologies of the modified surfaces were studied using atomic force microscope (AFM, Agilent 5500 model, USA) in tapping mode. X-ray photoelectron spectrum (XPS) was obtained on a K-Alpha X-ray photoelectron spectrometer (Thermo Fisher Scientific Co., USA). Ultraviolet–visible (UV–vis) absorption spectra were recorded on a Lambda 35 UV/VIS spectrometer (Perkin-Elmer instruments, USA). The static water contact angles were measured with a contact angle meter (Rame-Hart-100, USA) using droplets of deionized water at 25 °C. Electrochemical impedance spectroscopy (EIS) was carried out on a PGSTAT30/FRA2 system (Autolab, Netherlands) using the three-electrode setup in 0.1 M KCl containing 5 mM $Fe(CN)_6^{3-/4-}$ (1:1). The impedance spectra were recorded within the frequency range of 10^{-2} to 10^6 Hz. ^{1}H nuclear magnetic resonance (NMR) data were collected on Bruker ARX-300 spectrometer. Cyclic voltammetric and amperometric experiments were performed on a CHI 812B electrochemical workstation (CH Instruments Inc., USA). All experiments were carried out at room temperature using a conventional three-electrode system with a platinum disc electrode as working, a platinum wire as auxiliary, and a saturated calomel electrode as reference electrodes.

2.3. Preparation of PSSA-g-PPY/RGO composite

PSSA-g-PPY was synthesized by a reported procedure (Bae et al., 2005). First, for the preparation of pyrrolylmethylstyrene (PMS), 1 mL pyrrole reacted with 3 g KH for 6 h at room temperature under N_2, and 3 g CMS was then added to the solution and stirred at 0 °C for 12 h. The crude product was purified by column chromatography on silica gel eluting with n-hexane to give PMS. Second, for the synthesis of poly(sodium styrenesulfonate-co-pyrrolylmethylstyrene) (P(SSNa-co-PMS)), 10 g SSNa, 1 mL PMS, and 0.1 g azobisisobutyronitrile were dissolved in 120 mL dimethyl sulfoxide and then polymerized at 90 °C for 36 h under N_2 atmosphere. The product was precipitated into acetone, and filtered. Third, PSSA-g-PPY was prepared as follows: 1.0 g P(SSNa-co-PMS) was dissolved in 100 mL 1 M HCl solution, 0.1 mL pyrrole was added to the solution for 0.5 h under stirring, followed by dropwise addition of 50 mL 1 M HCl containing 0.03 M ammonium persulfate. After reaction at 0 °C for 6 h, a dark solution was obtained, filtered, and then concentrated in a vacuum evaporator and precipitated in acetone to get solid PSSA-g-PPY powder. ^{1}H NMR (300 MHz, D_2O) for PSSA-g-PPY: δ 7.50–6.50 (multiple peaks, Ar–H and pyrrole–H), δ 1.50 (single peak).

A 50 mL aqueous dispersion of graphene oxide (1 mg mL^{-1}) was sonicated for 60 min, and centrifuged (3000 rpm) to remove nonexfoliated GO sheets. Then 500 mg PSSA-g-PPY was added into the solution, and sonicated for 30 min to obtain the PSSA-g-PPY/GO dispersion. 500 μL of hydrazine was injected into the resulting solution and kept at 100 °C for 24 h. This dispersion was filtered through a filter membrane (0.2 μm pore size) to obtain a black solid, which was then collected and dried at 80 °C overnight to yield the PSSA-g-PPY/RGO nanocomposite.

2.4. Preparation of biosensor

Pt electrode (2 mm in diameter, CH Instruments, USA) was first polished to a mirror finish using 0.3 and 0.05 μm alumina slurries (Beuhler), followed by thorough rinsing with deionized water. 5 mg PSSA-g-PPY/RGO was added into 5 mL water and stirred for 2 h to obtain a PSSA-g-PPY/RGO suspension. 3 μL of the suspension, 2 mg mL^{-1} XnOx (in 0.05 M pH 7.0 PBS), and 0.5% PDDA were subsequently cast on the pretreated Pt electrode surface and allowed to dry under ambient conditions for 2 h after each drop-casting step. The formed PDDA membrane was used to fix the XnOx-impregnated PSSA-g-PPY/RGO composite on the electrode surface. Similarly, PSSA-g-PPY modified Pt electrodes were prepared.

2.5. Determination of hypoxanthine for fish freshness

A piece of fish meat (4–5 g) was homogenized in 15 mL of ultra-pure water for 30 min. The solution was then filtered through a filter membrane (0.2 μm pore size). Ultra-pure water was then added into the filtrate producing a total volume of 50 mL homogenized sample solution. A mixture containing equal volumes of the fish

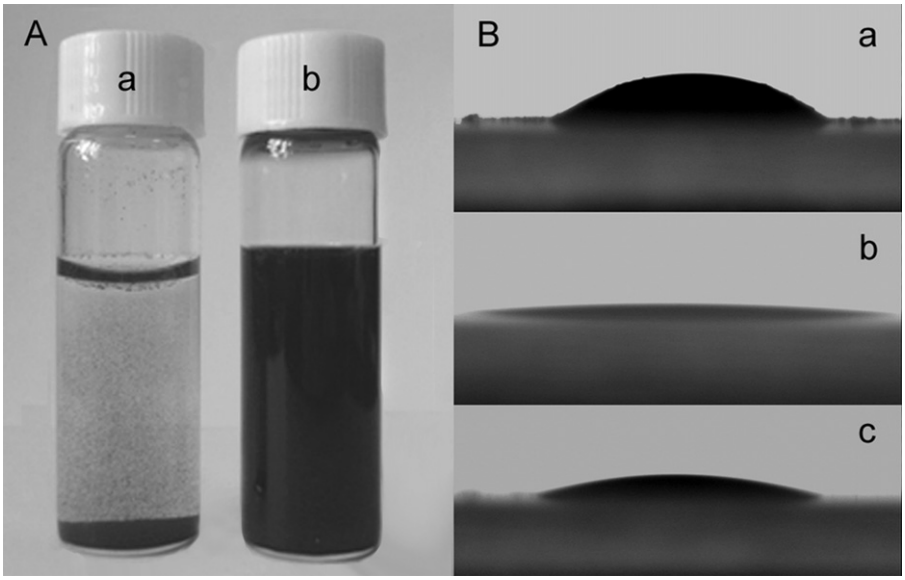

Fig. 1. (A) Photographs of water dispersions (1 mg mL^{-1}) of RGO (a) and PSSA-g-PPY functionalized RGO (b), and (B) contact angle photographs of RGO (a), PSSA-g-PPY (b) and PSSA-g-PPY/RGO (c) modified substrates.

extract and 0.1 M PBS was performed for fish freshness analysis. All sample solutions were prepared immediately for each experiment.

3. Results and discussion

3.1. Characterization of PSSA-g-PPY/RGO

PSSA-g-PPY/RGO nanocomposite was synthesized by chemically reducing the nanocomposite of GO and PSSA-g-PPY with hydrazine. The resulting PSSA-g-PPY/RGO could well disperse in water to produce a stable black solution for at least 2 months (Fig. 1A, photograph b). As control, the reduced GO dispersion without the presence of PSSA-g-PPY produced a RGO suspension, which quickly precipitated to the bottom of the bottle (Fig. 1A, photograph a). The solubility of PSSA-g-PPY/RGO was determined to be about 3.0 mg mL^{-1} according to the saturated amount in water (Zhang et al., 2006).

The biocompatibility of PSSA-g-PPY/RGO was characterized with the contact angle measurements. As shown in Fig. 1B, the contact angles of RGO (photograph a), PSSA-g-PPY (photograph b) and PSSA-g-PPY/RGO (photograph c) films were measured to be 47°, about 0° and 17°, respectively. The PSSA-g-PPY copolymer showed the minimum contact angle, which was contributed to the sulfonic acid groups introduced by water-soluble PSSA. Compared with bare RGO, the PSSA-g-PPY/RGO exhibited much smaller contact angle, indicating good hydrophilicity or biocompatibility. The improved hydrophilicity and biocompatibility of the nanocomposite could greatly enhance the loading capacity of protein and preserve the bioactivity of the immobilized biomolecules, thus provided a desirable platform for biosensing and biocatalytic application.

Fig. 2 shows the AFM images of GO and PSSA-g-PPY/RGO. The samples used for AFM studies were prepared by depositing the corresponding dispersions on mica surfaces and dried at room temperature. The cross-sectional view of the typical AFM image of the exfoliated GO (Fig. 2A) indicated that the average thickness of GO sheets is about 0.85 nm. In the case of PSSA-g-PPY coated RGO, the average thickness was about 2.8 nm (Fig. 2B). The obvious increase in thickness and the relatively uniform thickness suggested that the surface of RGO was coated with the copolymer due to the strong interfacial interactions between PSSA-g-PPY and RGO.

XPS was employed to analyze the GO and PSSA-g-PPY/RGO. The C 1s XPS spectrum of GO (Fig. 3A) indicated the presence of 4 types of carbon bonds: C–C (284.5 eV), C–O (286.6 eV), C=O (288.1 eV), and O–C=O (289.3 eV) (Bai et al., 2009). After reduction, the peak associated with C–C (284.5 eV) became predominant, while the peaks related to the oxidized carbon species were greatly weakened (Fig. 3B). Furthermore, additional peaks assigned to C–S (285.6 eV) and C–N, C=N (286.2 eV) species of PSSA-g-PPY appeared in the spectrum of PSSA-g-PPY/RGO. These results demonstrated that GO was reduced into RGO, and PSSA-g-PPY was coated onto the graphene sheets.

UV–vis absorption spectra of RGO, PSSA-g-PPY and PSSA-g-PPY/RGO were shown in Fig. 3C. No absorption peak for RGO sample was observed in the wavelength range of 300–1300 nm (curve a) (Liu et al., 2009a). The UV–vis spectrum of PSSA-g-PPY (curve b) showed a bipolaron absorption at 450 nm and a free carrier tailing of anti-bipolaron absorption in the near-IR region with a maximum value at about 1110 nm, indicating that the copolymer was in a self-doped state (Bae et al., 2005; Antony and Jayakannan, 2007). After integrating with RGO, the characteristic absorption peaks at 450 and 1110 nm arising from PSSA-g-PPY were blue shifted to 415 and 965 nm in the spectra of PSSA-g-PPY/RGO (curve c), and the absorption peak at 415 nm was more broaden. These results suggested the nanocomposite was formed via the π–π noncovalent interaction between the ring of PSSA-g-PPY copolymer and the planar structure of the RGO (Star et al., 2001; Wu and Lin, 2006; Geng et al., 2008).

3.2. Electrochemical characterization of PSSA-g-PPY/RGO

Fig. 4A shows the electrochemical behaviors of the immobilized PSSA-g-PPY/RGO in 0.05 M pH 7.0 PBS. Compared with bare Pt electrode (curve a), the cyclic voltammograms (CVs) of both PSSA-g-PPY (curve b) and PSSA-g-PPY/RGO modified electrodes (curve c) exhibited a pair of well defined redox peaks corresponding to the electrochemical reduction and oxidation of PPY (Zhang et al., 2008). The peak currents of PSSA-g-PPY/RGO modified electrode were much higher than those of PSSA-g-PPY modified electrode in neutral aqueous medium, which should be contributed to the fast electron transfer and high specific surface area of RGO for loading of PSSA-g-PPY. In addition, PSSA-g-PPY was unstable

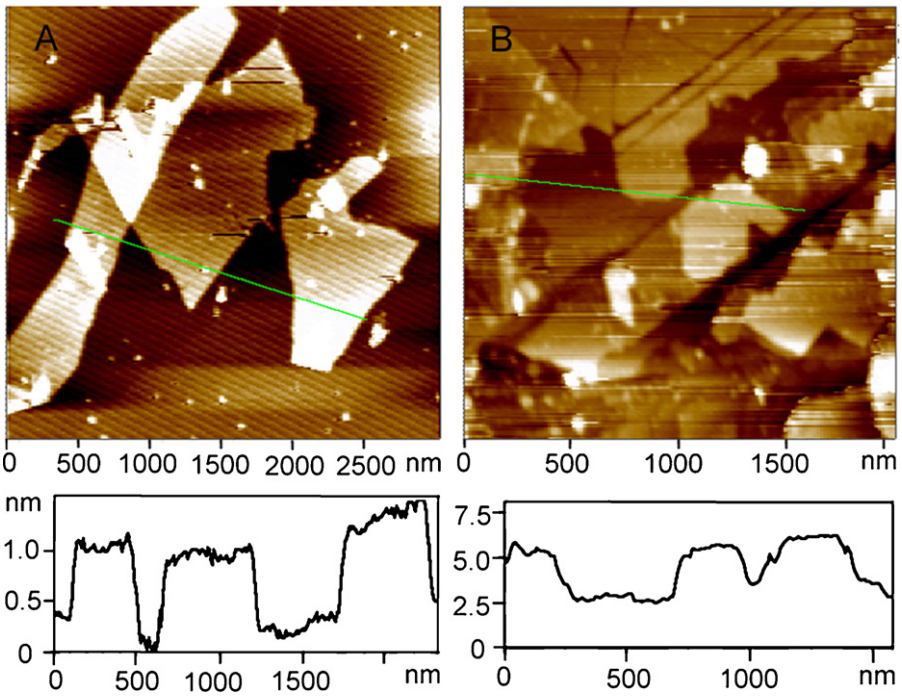

Fig. 2. AFM images of (A) GO and (B) PSSA-g-PPY/RGO on mica.

and easily lost from the electrode surface, while the immobilized PSSA-g-PPY/RGO was quite stable at electrode surface due to the formation of a crosslinked 3-dimensional network between PSSA-g-PPY chains and the basal planes of graphene. The as-prepared modified electrode could greatly improve the electrochemical signal transduction in bioanalysis.

Using $Fe(CN)_6^{3-/4-}$ redox couple as the electrochemical probe, the Nyquist plots of different electrodes in the frequency range from 10^{-2} to 10^6 were shown in Fig. 4B. At bare Pt electrode the redox process of the probe showed an electron transfer resistance of about 65 Ω (curve a). After the PSSA-g-PPY copolymer was coated on the electrode, the resistance increased to about 105 Ω (curve b), suggesting that the PSSA-g-PPY copolymer slightly blocked the electron transfer between the redox probe and electrode surface. However, the PSSA-g-PPY/RGO modified electrode showed the lowest resistance for the redox probe (curve c), further implying that PSSA-g-PPY/RGO composite was an excellent electric conducting material.

3.3. Response to oxidation of H_2O_2 and UA

The reliable, accurate, and rapid determination of H_2O_2, a product of enzymatic reaction, is of practical importance because it is an essential mediator in food, pharmaceutical, clinical, industrial, and environmental analyses (Wang, 2008; Zhou et al., 2009). Bare Pt electrode exhibited a good response to H_2O_2 at +0.42 V (Fig. 4C, curve a). When PSSA-g-PPY was modified on the electrode, the peak current decreased (Fig. 4C, curve b), which suggested that PSSA-g-PPY had a blocking effect on the electron exchange between H_2O_2 and the electrode surface. However, an enhanced peak current was observed at PSSA-g-PPY/RGO modified electrode, and the anodic potential shifted negatively to +0.39 V (Fig. 4C, curve c), which was much lower than +0.5 V at polyelectrolyte multilayer films modified Pt electrode (Hoshi et al., 2001). This means that the PSSA-g-PPY/RGO modified electrode has higher electrocatalytic activity toward oxidation of H_2O_2, which is in favor of the preparation of enzyme-based sensor.

UA could be oxidized at +0.52 V at bare Pt electrode (Fig. 4D, curve a). With coating of PSSA-g-PPY on the electrode surface, the current decreased, however, the anodic peak potential shifted negatively to +0.45 V (Fig. 4D, curve b), indicating the electrocatalytic activity of PSSA-g-PPY for the oxidization of UA. The PSSA-g-PPY/RGO modified electrode exhibited an increasing current with a negative shift of anodic potential to +0.38 V (Fig. 4D, curve c), which was lower than +0.55 V at a fluorosurfactant-modified platinum electrode (Chen and Zu, 2007). These results revealed that the

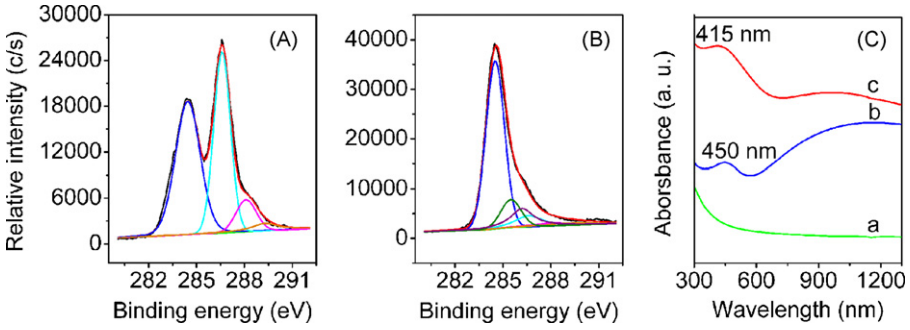

Fig. 3. C 1s XPS spectra of (A) GO and (B) PSSA-g-PPY/RGO, and (C) UV–vis absorption spectra of RGO (a), PSSA-g-PPY (b) and PSSA-g-PPY/RGO (c).

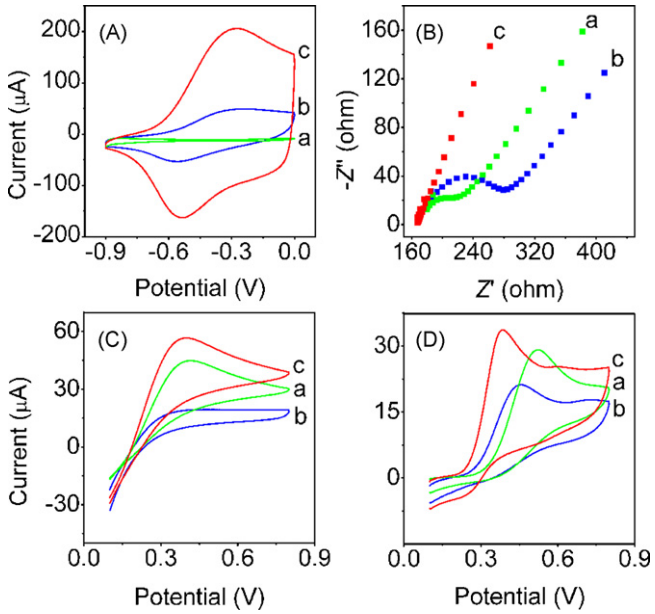

Fig. 4. (A) Cyclic voltammograms in pH 7.0 PBS, (B) EIS in 0.1 mM KNO_3 containing 5 mM $K_3[Fe(CN)_6]/K_4[Fe(CN)_6]$, and the electrocatalytic oxidation of (C) 3.0 mM H_2O_2 and (D) 3.0 mM uric acid in 0.05 M pH 7.0 PBS at bare (a), PSSA-g-PPY modified (b) and PSSA-g-PPY/RGO modified Pt electrode (c). Scan rate: 100 mV s^{-1}.

as-prepared hybrid nanocomposite possessed good electrocatalytic activity toward oxidation of both H_2O_2 and UA.

3.4. Amperometric performance of XnOx/PSSA-g-PPY/RGO modified electrode

Similarly, XnOx/PSSA-g-PPY/RGO modified electrode also showed sensitive response to the oxidations of both H_2O_2 and UA. Upon addition of hypoxanthine to air-saturated PBS in absence of both H_2O_2 and UA, a rapid increase in the anodic current appeared as a result of the oxidations of H_2O_2 and UA produced from the enzymatic reactions:

$$\text{Hypoxanthine} + O_2 \xrightarrow{\text{XnOx}} \text{Xanthine} + H_2O_2$$

$$\text{Xanthine} + O_2 \xrightarrow{\text{XnOx}} \text{Uric acid} + H_2O_2$$

Therefore, the determination of hypoxanthine in this single sensing element could be achieved by measuring the oxidation current of H_2O_2 and UA at XnOx/PSSA-g-PPY/RGO modified electrode.

The dependence of the amperometric response of the biosensor on the applied potential was investigated over the range of +0.3–0.8 V in this work. The amperometric response of resulting biosensor to 5 μM hypoxanthine increased with the increasing potential from +0.3 to 0.55 V and tended to a stable response after +0.55 V. Therefore, +0.55 V was an optimal applied potential for amperometric measurement.

The pH value of the detection solution also affected the amperometric response of the biosensor. The current increased as the pH changed from 5.0 to 7.0, following with a fast decrease in the pH range of 7.0–8.0. The maximum response was obtained at pH 7.0, which was consistent with the optimum pH for the free XnOx (Shan et al., 2009). This indicated that the immobilization procedure did not alter the optimum pH of XnOx. Therefore, pH 7.0 PBS was used as the electrolyte in further work.

The steady-state amperometric response of the XnOx/PSSA-g-PPY/RGO modified electrode to hypoxanthine was determined by the successive addition of hypoxanthine into 10 mL PBS under the optimum conditions (Fig. 5). After the addition of hypoxanthine, the

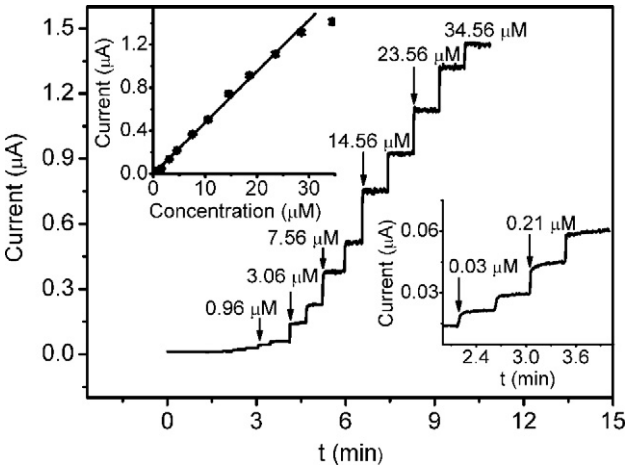

Fig. 5. Typical current–time response curve of the biosensor upon successive additions of hypoxanthine with marked concentrations. Upper inset: linear calibration curve. Lower inset: amplified response curve at low concentrations. Applied potential: +0.55 V.

anodic current immediately increased and reached 95% of steady-state current within 5 s. The linear concentration range was from 3×10^{-8} M to 2.8×10^{-5} M with a correlation coefficient of 0.999, a high sensitivity of 673 ± 4 μA M^{-1} cm^{-2} and a detection limit of 10 nM at the signal-to-noise ratio of 3. The performance of the biosensor was better than those of ruthenium purple-mediated biosensor with a linear range from 2×10^{-7} M to 4×10^{-5} M and a sensitivity of 334 μA M^{-1} cm^{-2} (Tian et al., 2007), electrochemiluminescent biosensor with a linear range from 8.0×10^{-6} M to 3.0×10^{-4} M and a detection limit of 3 μM (Lin et al., 2008), and gold nanoparticle-based amperometric biosensor with a linear range from 5.0×10^{-6} to 1.5×10^{-4} M (Cubukcu et al., 2007). To our best knowledge, this was the lowest detection limit of electrochemical biosensors for hypoxanthine. The good performance could be attributed to the enhanced electrocatalytic activity and good biocompatibility of PSSA-g-PPY/RGO nanocomposite.

The repeatability of the XnOx/PSSA-g-PPY/RGO modified electrode was examined at the hypoxanthine concentrations of 0.05 and 5 μM, and the relative standard deviations for six determinations were 3.4% and 2.2%, respectively. In addition, the relative standard deviation of current signals for measurement of 5 μM hypoxanthine at six independently prepared biosensors was 2.6%, which proved good reproducibility of the biosensor preparation. The long-term stability of the XnOx/PSSA-g-PPY/RGO modified electrode was investigated in two ways. The enzyme electrode retained 94% of its original response after 4 weeks storage in 0.05 M pH 7.0 PBS at 4 °C. At the same storage condition, when used once per 4 days, the enzyme electrode retained 96%, 94%, 92%, 90%, 87%, 84% and 81% of its initial activity after 4, 8, 12, 16, 20, 24 and 28 days, respectively. These results indicated acceptable stability.

3.5. Analysis of fish samples

Hypoxanthine is the major mutability of adenine nucleotide degradation that accumulating in fish continuously after death. The determination of fish quality is reflected directly by increase in hypoxanthine concentration (Yano et al., 1995; Shan et al., 2009). Here the XnOx/PSSA-g-PPY/RGO sensing system was used to estimate the freshness of fish. Due to the lack of experimental conditions available to perform a traditional or referee determination, recovery testing was carried out to demonstrate the validity of the proposed method (Table 1). After fish was killed and stored for 0, 4, 12 and 24 h at room temperature, the concentration of

Table 1
Determination of hypoxanthine in fish samples ($n = 3$).

Sample	Store condition	Added (μM)	Found (μM)	Recovery (%)
1	Freshly killed	0	5.55 ± 0.03	
		10	14.93 ± 0.04	93.8 ± 0.4
2	4 h after death	0	5.83 ± 0.04	
		10	15.32 ± 0.07	94.9 ± 0.7
3	12 h after death	0	9.05 ± 0.08	
		10	18.55 ± 0.20	95.0 ± 2
4	24 h after death	0	15.28 ± 0.12	
		10	24.92 ± 0.20	96.4 ± 2

hypoxanthine increased, and the obtained recoveries were more than (93.8 ± 0.4)%, indicating acceptable accuracy.

4. Conclusions

A biocompatible PSSA-g-PPY/RGO nanocomposite was designed by functionalizing the graphene sheets with conducting graft copolymer via π–π noncovalent interaction. The copolymer exhibited water-solubilization and high conductivity. The resulting PSSA-g-PPY/RGO nanocomposite showed uniform sheet nanostructure and could disperse in water to form a stable solution. The hybrid nanocomposite possessed excellent electrocatalytic activity toward electrooxidation of both H_2O_2 and UA. Based on the electrocatalysis activity, a biosensor was constructed for fast detection of hypoxanthine by an enzymatic cycle. The biosensor showed wide linear range, low detection limit, good reproducibility and accepted long-term stability, and could successfully detect hypoxanthine in fish samples. The copolymer opens an insight for functionalization of graphene sheets, and has a great potential for multiple applications in electronic devices.

Acknowledgements

This research was financially supported by National Basic Research Program of China (2010CB732400), the National Science Funds for Creative Research Groups (20821063), the Major Research Plan (90713015) and General Programs (20875044, 20705012) from National Natural Science Foundation of China, and Natural Science Foundation of Jiangsu (BK2008014).

References

Antony, M.J., Jayakannan, M., 2007. J. Phys. Chem. B 111, 12772–12780.
Bae, W.J., Kim, K.H., Jo, W.H., Park, Y.H., 2005. Macromolecules 38, 1044–1047.
Bai, H., Xu, Y.X., Zhao, L., Li, C., Shi, G.Q., 2009. Chem. Commun., 1667–1669.
Causse, E., Pradelles, A., Dirat, B., Negre-Salvayre, A., Salvayre, R., Couderc, F., 2007. Electrophoresis 28, 381–387.
Chao, S., Wrighton, M.S., 1987. J. Am. Chem. Soc. 109, 2197–2199.
Chen, Z.F., Zu, Y.B., 2007. J. Electroanal. Chem. 603, 281–286.
Cubukcu, M., Timur, S., Anik, U., 2007. Talanta 74, 434–439.
Du, D., Zou, Z.X., Shin, Y.S., Wang, J., Wu, H., Engelhard, M.H., Liu, J., Aksay, I.A., Lin, Y.H., 2010. Anal. Chem. 82, 2989–2995.
Farthing, D., Sica, D., Gehr, T., Wilson, B., Fakhry, I., Laru, T., Farthing, C., Karnes, H.T., 2007. J. Chromatogr. B 854, 158–164.
Geim, A.K., 2009. Science 324, 1530–1534.
Geng, J.X., Kong, B.S., Yang, S.B., Youn, S.C., Park, S., Joo, T.H., Jung, H.T., 2008. Adv. Funct. Mater. 18, 2659–2665.
Holcombe, T.W., Woo, C.H., Kavulak, D.F.J., Thompson, B.C., Frechet, J.M.J., 2009. J. Am. Chem. Soc. 131, 14160–14161.
Hoshi, T., Saiki, H., Kuwazawa, S., Tsuchiya, C., Chen, Q., Anzai, J., 2001. Anal. Chem. 73, 5310–5315.
Hummers, W.S., Offeman, R.E., 1958. J. Am. Chem. Soc. 80, 1339–11339.
Kang, X.H., Wang, J., Wu, H., Aksay, I.A., Liu, J., Lin, Y.H., 2009. Biosens. Bioelectron. 25, 901–905.
Kim, Y.R., Bong, S., Kang, Y.J., Yang, Y., Mahajan, R.K., Kim, J.S., Kim, H., 2010. Biosens. Bioelectron. 25, 2366–2369.
Kong, Y.T., Boopathi, M., Shim, Y.B., 2003. Biosens. Bioelectron. 19, 227–232.
Li, D., Muller, M.B., Gilje, S., Kaner, R.B., Wallace, G.G., 2008a. Nat. Nanotechnol. 3, 101–105.
Li, X.L., Wang, X.R., Zhang, L., Lee, S.W., Dai, H.J., 2008b. Science 319, 1229–1232.
Li, X.S., Zhu, Y.W., Cai, W.W., Borysiak, M., Han, B.Y., Chen, D., Piner, R.D., Colombo, L., Ruoff, R.S., 2009. Nano Lett. 9, 4359–4363.
Liu, H., Gao, J., Xue, M.Q., Zhu, N., Zhang, M.N., Cao, T.B., 2009a. Langmuir 25, 12006–12010.
Liu, J.B., Li, Y.L., Li, Y.M., Li, J.H., Deng, Z.X., 2010. J. Mater. Chem. 20, 900–906.
Liu, Q., Liu, Z.F., Zhang, X.Y., Yang, L.Y., Zhang, N., Pan, G.L., Yin, S.G., Chen, Y.S., Wei, J., 2009b. Adv. Funct. Mater. 19, 894–904.
Lin, Z.Y., Sun, J.J., Chen, J.H., Guo, L., Chen, Y.T., Chen, G.N., 2008. Anal. Chem. 80, 2826–2831.
Patil, A.J., Vickery, J.L., Scott, T.B., Mann, S., 2009. Adv. Mater. 21, 3159–3164.
Rao, C.N.R., Sood, A.K., Subrahmanyam, K.S., Govindaraj, A., 2009. Angew. Chem. Int. Ed. 48, 7752–7777.
Robinson, J.T., Perkins, F.K., Snow, E.S., Wei, Z.Q., Sheehan, P.E., 2008. Nano Lett. 8, 3137–3140.
Shan, C.S., Yang, H.F., Han, D.X., Zhang, Q.X., Ivaska, A., Niu, L., 2010. Biosens. Bioelectron. 25, 1504–1508.
Shan, D., Wang, Y.N., Xue, H.G., Cosnier, S., 2009. Sens. Actuators B: Chem. 136, 510–515.
Si, Y.C., Samulski, E.T., 2008. Nano Lett. 8, 1679–1682.
Stankovich, S., Dikin, D.A., Dommett, G.H.B., Kohlhaas, K.M., Zimney, E.J., Stach, E.A., Piner, R.D., Nguyen, S.T., Ruoff, R.S., 2006a. Nature 442, 282–286.
Stankovich, S., Dikin, D.A., Piner, R.D., Kohlhaas, K.A., Kleinhammes, A., Jia, Y.Y., Wu, Y., Nguyen, S.T., Ruoff, R.S., 2007. Carbon 45, 1558–1565.
Stankovich, S., Piner, R.D., Chen, X.Q., Wu, N.Q., Nguyen, S.T., Ruoff, R.S., 2006b. J. Mater. Chem. 16, 155–158.
Star, A., Stoddart, J.F., Steuerman, D., Diehl, M., Boukai, A., Wong, E.W., Yang, X., Chung, S.-W., Choi, H., Heath, J.R., 2001. Angew. Chem. Int. Ed. 40, 1721–1725.
Subrahmanyam, K.S., Ghosh, A., Gomathi, A., Govindaraj, A., Rao, C.N.R., 2009. Nanosci. Nanotechnol. Lett. 1, 28–31.
Tian, F.M., Llaudet, E., Dale, N., 2007. Anal. Chem. 79, 6760–6766.
Venugopal, V., 2002. Biosens. Bioelectron. 17, 147–157.
Wang, D.W., Li, F., Zhao, J.P., Ren, W.C., Chen, Z.G., Tan, J., Wu, Z.S., Gentle, I., Lu, G.Q., Cheng, H.M., 2009. ACS Nano. 3, 1745–1752.
Wang, 2008. J. Chem. Rev. 108, 814–825.
Widge, A.S., Jeffries-El, M., Cui, X.Y., Lagenaur, C.F., Matsuoka, Y., 2007. Biosens. Bioelectron. 22, 1723–1732.
Wu, T.M., Lin, S.H., 2006. J. Polym. Sci., Part A: Polym. Chem. 44, 6449–6457.
Xu, Y.X., Bai, H., Lu, G.W., Li, C., Shi, G.Q., 2008. J. Am. Chem. Soc. 130, 5856–5857.
Yang, H.F., Shan, C.S., Li, F.H., Han, D.X., Zhang, Q.X., Niu, L., 2009. Chem. Commun., 3880–3882.
Yang, X.Y., Dou, X., Rouhanipour, A., Zhi, L.J., Rader, H.J., Mullen, K., 2008. J. Am. Chem. Soc. 130, 4216–4217.
Yano, Y., Kataho, N., Watanabe, M., Nakamura, T., Asano, Y., 1995. Food Chem. 52, 439–445.
Yoon, H., Jang, J., 2009. Adv. Funct. Mater. 19, 1567–1576.
Zhang, H., Li, H.X., Cheng, H.M., 2006. J. Phys. Chem. B 110, 9095–9099.
Zhang, H., Zhong, X., Xu, J.J., Chen, H.Y., 2008. Langmuir 24, 13748–13752.
Zhong, Z.Y., Wu, W., Wang, D., Wang, D., Shan, J.L., Qing, Y., Zhang, Z.M., 2010. Biosens. Bioelectron. 25, 2379–2383.
Zhou, M., Zhai, Y.M., Dong, S.J., 2009. Anal. Chem. 81, 5603–5613.
Zhu, Y., Higginbotham, A.L., Tour, J.M., 2009. Chem. Mater. 21, 5284–5291.